Paper # 087LF-0020 **Topic: Laminar Flame**

Western States Section of the Combustion Institute
California Institute of Technology
March 23-25, 2014.

Non-linear Extrapolation of Laminar Flame Properties from Spherically Expanding Flames

S. Coronel[1], *N. Bitter*[1], *V. Thomas* [2], *R. Mevel*[*1], *J.E. Shepherd*[1]

[1]*Graduate Aeronautics Laboratory (GALCIT),*
California Institute of Technology, Pasadena, California 91125, USA
[2]*Mechanical Engineering,*
Johns Hopkins University, Baltimore, MD 21218

The spherically expanding flame is a useful configuration for experimentally measuring laminar flame speeds and Markstein lengths. Although these parameters are often fitted to the data linearly, for highly stretched flames it can be necessary to employ a fitting procedure that accounts for nonlinearity of the relationship between flame speed and stretch rate. This paper assesses the performance of such methods by generating sets of synthetic data and then attempting to recover the laminar flame speed and Markstein length using a nonlinear fit. The method used in this paper fits the laminar flame properties by minimizing the difference between the data points and a simulated flame trajectory, using a non-linear least squares method to accomplish the minimization. It is found that the least squares error, which is to be minimized, is a weak function of the Markstein length and exhibits a shallow minimum, especially for noisy data. This can lead to substantial error in the fitted value of the Markstein length; for instance, 2% noise in the flame radius data produces about 20% relative error in the fitted Markstein length. The initial and final flame radii as well as the number of points in the experimental data set are found to have only a small influence on the results. However, the results are sensitive to the initial guesses that are used to start the least squares minimization. Finally we observe that for positive Markstein length there is an upper limit to the nonlinear relationship between flame speed and stretch, and fitting can become inaccurate near this limit. Despite these difficulties, the nonlinear fitting approach performs considerably better than linear ones for highly stretched flames.

1 Introduction

Laminar flame properties such as the laminar burning speed and the Markstein length are important fundamental parameters for a wide number of combustion applications including spark ignition engines [1] and gas turbines [2]. Knowledge of the laminar burning speed is also important in modeling turbulent combustion since the turbulent burning speed is often modeled as a function of the laminar burning speed [3, 4]. The laminar burning speed is defined as the normal propagation velocity of fresh gas relative to a fixed, planar flame front; it is frequently measured experimentally using spherically expanding flames [5–7]. Figure 1 shows examples of spherical flame propagation in hydrogen-based mixtures. The presence of flame stretch in such experiments precludes direct measurement of the laminar burning velocity [9]. Instead, the measured flame velocity must be extrapolated to conditions of zero stretch. Markstein first proposed this correction to the burning speed by introducing a parameter now known as the Markstein length [10], which characterizes the response of the flame to stretch. Asymptotic theoretical analysis [11–13] performed in the limit

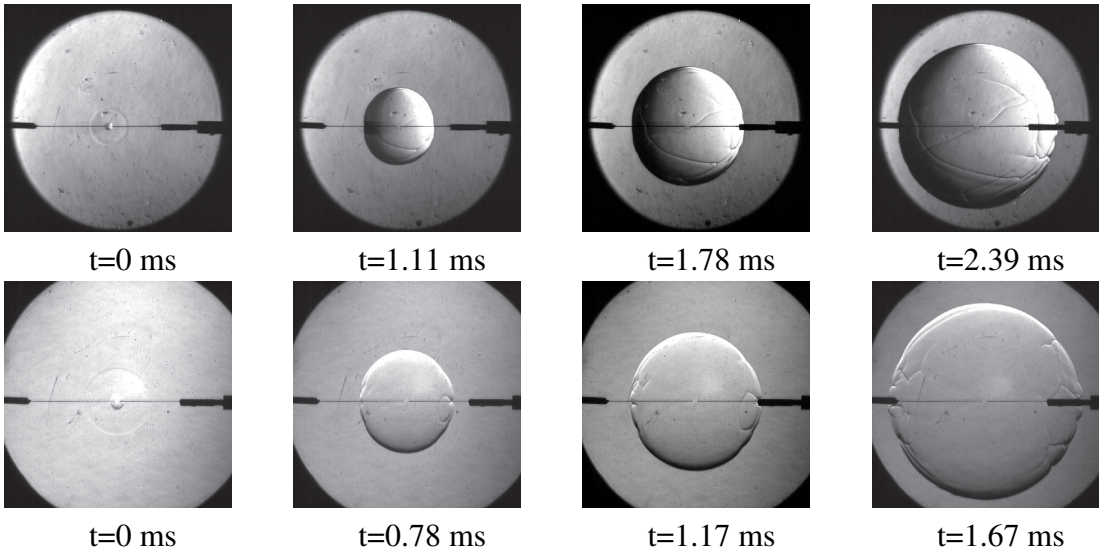

Figure 1: Examples of flame propagation sequences in a H_2-air mixture (top) and a H_2-N_2O mixture [8] (bottom) obtained with schlieren visualization. Initial conditions: H_2-air mixture: Φ=1.5 ; P_1=100 kPa; T_1=295 K. H_2-N_2O mixture: Φ=0.6 ; P_1=20 kPa; T_1=295 K.

of high activation energy and low stretch rate have related the stretched and unstretched burning speeds through a linear relationship. This approach has been applied extensively during the past 20 years to extract the laminar burning speed from experimental data [8, 14–17]. Further theoretical work by Ronney and Sivashinsky [18] has led to a non-linear relationship between the stretched and the unstretched burning speed which has been used by a number of groups in the past few years to account for non-linear effects of stretch on the flame propagation [19–23]. Comparison of the results obtained through linear and non-linear extrapolations demonstrated that both the burning speed and Markstein length can be poorly estimated by the linear method for mixtures that are away from the stoichiometry [19, 20]. In order to account for the non-linear effects of stretch without performing numerical differentiation of the experimental data, Kelley and Law [19] analytically integrated the expression of Ronney and Sivashinsky [18]. Halter et al. [20] also evaluated this latter methodology for methane-air burning speed measurements and reported a strong sensitivity to the initial guesses required to obtained the flame parameters.

This study seeks to evaluate the performance of nonlinear fitting methods by extracting the laminar flame properties from synthetic data sets. We investigate the sensitivity of the results to experimental parameters like initial and final flame radius, the number of points in the data set, and measurement noise, as well as numerical parameters like the initial guess that is used to start the nonlinear fit. First, the linear and non-linear approaches are reviewed and the limits of applicability of the relationship between flame speed and stretch rate are discussed. Then the present nonlinear fitting procedure is described and the performance of the method is evaluated.

2 Methodologies to extract flame properties

2.1 Linear methodology

Asymptotic theoretical analysis by Sivashinsky [11], Matalon and Matkowsky [12] and Clavin [13], performed in the limit of high activation energy, reveals a linear relation between the stretched and unstretched burning speeds in the low stretch rate regime

$$S_L = S_L^0 - L_B^{'} \cdot K. \tag{1}$$

Here S_L and S_L^0 are the stretched and the unstretched laminar burning speeds, $L_B^{'}$ is the unburnt gas Markstein length and K is the stretch rate. Karlovitz et al. [24] expressed the stretch rate in terms of the normalized rate of change of an elementary flame front area as

$$K = \frac{1}{A} \cdot \frac{dA}{dt}, \tag{2}$$

where A the flame front area. In the case of a spherical flame, the flame surface is given by

$$A = 4 \cdot \pi \cdot R_f^2, \tag{3}$$

which leads to the following expression for the stretch rate [7, 9, 14, 17]:

$$K = 2 \cdot \frac{V_S}{R_f}, \tag{4}$$

given that the stretched spatial velocity, or the flame speed, V_S, corresponds to the flame radius increase rate

$$V_S = \frac{dR_f}{dt}. \tag{5}$$

In the case of a large volume vessel and for measurements limited to the initial period of propagation where the flame radius is small, the pressure increase can be neglected [25], so that the burning speed and the spatial velocity are linked only through the expansion ratio across the flame front

$$S_L = \frac{V_S}{\sigma}. \tag{6}$$

where σ is the expansion ratio defined as

$$\sigma = \frac{\rho_u}{\rho_b}, \tag{7}$$

and ρ_u and ρ_b are the unburnt and burnt gas densities, respectively. Combining Equation 1 and Equation 6, the stretched and unstretched flame speed can be linked

$$V_S = V_S^0 - L_B \cdot K, \tag{8}$$

where L_B=$L_B^{'}/\sigma$. Using the experimental evolution of the flame radius as a function of time, the local flame velocity as well as the local stretch rate can be derived and the unstretched flame speed obtained by linearly extrapolating to zero stretch. As a part of this procedure one must fit the

$R_f = f(t)$ data, usually with a high order polynomial, and differentiate the fitted curve in order to obtain a smooth evolution of the flame speed as a function of stretch. The main limitation of this procedure arises from the differentiation which introduce artificial noise that can lead to misleading results.

Another way to proceed is to substitute Equation 4 and Equation 6 into Equation 1, and integrate with respect to time, which produces an expression for the unstretched spatial flame velocity as a function of time and flame radius

$$V_S^0 \cdot (t^i - t) = R_f^i - R_f + 2 \cdot L_B \cdot \ln\left(\frac{R_f}{R_f^i}\right) + Cst \tag{9}$$

Here the superscript i designates the i^{th} data point in a set of experimental measurements, and Cst is an integration constant. Using Equation 9, a least square fitting procedure can be applied to an experimental set of $R_f = f(t)$ data provided that $R_f \ll D_{exp}$, where D_{exp} is the characteristic dimension of the experimental set-up. The unstretched flame velocity and the Markstein length are determined from this procedure as the coefficients of the linear fit.

2.2 Non-linear methodology

By removing the assumption of a linear relationship between the stretched and the unstretched flame speeds, Ronney and Sivashinsky [11] obtained the nonlinear result:

$$\left(\frac{V_S}{V_S^0}\right)^2 \ln\left(\frac{V_S}{V_S^0}\right)^2 = -2\frac{\sigma L_B K}{V_S^0} \tag{10}$$

This expression can be used directly to derive both the flame speed and the Markstein length, but in doing so one must fit the $R_f = f(t)$ data with polynomials and differentiate to determine V_s, as was done by Halter et al. [20] and Bouvet et al. [22].

In order to avoid differentiating the experimental data, Kelley and Law [19] proposed an integral form of Equation 10

$$t = A\left[E_1\left(\ln \xi^2\right) - \frac{1}{\xi^2 \ln \xi}\right] + C \tag{11}$$

where

$$A = \frac{2\sigma L_B}{V_S^0}, \tag{12}$$

$$R_f = -\frac{2\sigma L_B}{\xi \ln \xi}, \tag{13}$$

$$E_1(x) = \int_x^\infty \frac{e^{-z}}{z} dz, \tag{14}$$

and C is a constant of integration. The parameter ξ, which is the ratio of the stretched to unstretched flame speed, falls in the range $[e^{-1}, 1)$ for $L_B > 0$ and $[1, \infty)$ for $L_B < 0$. The parameters, A, L_B,

and C can be determined using non-linear least-squares fitting, that is, minimizing the expression

$$E_R = \frac{1}{N}\left[\sum_{i=0}^{N}\left(t^i - A\left[E_1\left(\ln\xi_i^2\right) - \frac{1}{\xi_i^2\ln\xi_i}\right] - C\right)^2\right]^{1/2} \tag{15}$$

where the summation on i is taken over all measured values of flame radius and time. The unstretched flame speed can then be deduced from the values of A and L_B that minimize Equation 15.

3 Analysis of the Ronney-Sivashinsky non-linear equation

The nonlinear method of flame speed extraction described in section 2 relies on the quasi-steady relationship between flame speed and stretch rate given by Equation 10. However, this equation has solutions only for certain values of the ratio $\sigma L_B/R_f$. To demonstrate this, one can combine Equation 4 with Equation 10 and simplify the logarithmic term to obtain the relation

$$\frac{V_S}{V_S^0}\cdot\ln\left(\frac{V_S}{V_S^0}\right) = -2\frac{\sigma L_B}{R_f}\,. \tag{16}$$

Since the burning velocity is positive, the term on the left hand side may take on values only within the range $[-e^{-1},\infty)$. For $L_B<0$ there is one solution for all positive values of R_f, but for $L_B>0$ there are solutions only if

$$\frac{R_f}{2\sigma L_B} \geq e \qquad\qquad (L_B>0) \tag{17}$$

Thus for positive Markstein length there exists a minimum flame radius below which the quasi-steady relationship between flame speed and stretch rate is not valid, and hence the laminar flame speed cannot be extracted using Equation 10. This constraint can also be viewed as a maximum Markstein length, $L_{B,max}$, for fixed flame radius. The fact that no solutions exist for small flame radii is a consequence of the neglected unsteady term, which is important in the early flame dynamics [11].

When extracting laminar flame properties from experimental data, one can apply the methods of section 2 only for data points having large enough flame radii to satisfy Equation 17. Data points which do not satisfy this criterion do not conform to the model equation, Equation 10, and thus may lead to a poor quality of fit (large residuals) or erroneous fitted values of V_s^0 and L_B. Unfortunately, the limitation given by Equation 17 depends on the Markstein length, which is itself one of the unknowns being sought. In practice one must initially select the experimental data points based on an estimate of L_B and confirm after fitting the data that Equation 17 was indeed satisfied, revising the set of included data points if necessary.

4 Description of the present approach

The majority of previous studies [20, 26] that have studied the accuracy of the linear and nonlinear methods for flame parameters extraction have used experimental data. A difficulty of this approach is that the exact flame speed and Markstein length are not known a priori and depend on the

method used to obtain them. Another approach is to use synthetic data, as was done by Chen [27]. However, Chen generated his reference data using detailed numerical simulations which limits the number of synthetic samples that can be generated because of the high computational cost of such simulations. In this paper, synthetic data is generated instead by numerically integrating the flame radius as a function of time, evaluating the flame speed at each time step using Equation 16.

The present method for extracting L_B and V_S^0 uses non-linear least squares regression to determine the values of L_B and V_S^0 that minimize the difference between the experimentally measured flame radius, R_f^i, and an ideal flame spherical flame radius, $R_{f,calc}^i$, which represents the evolution of spherical flame in the absence of noise and measurement error for a flame that obeys Equation 16. The values of L_B and V_S^0 are extracted by minimizing the residual function,

$$E_R = \frac{1}{N}\left[\sum_{i=1}^{N}\left(\frac{R_f^i - R_{f,calc}^i}{R_f^i}\right)^2\right]^{1/2} \tag{18}$$

The first step in the process is to generate an idealized set of data points, t^i vs. $R_{f,calc}^i$, by integrating Equation 16. The initial conditions, t^0 and R_f^0, are determined from the data set to be fitted. The values of L_B and V_S^0 are then iteratively refined until Equation 18 is minimized. The numerical integration of Equation 16 is carried out using the Matlab ODE solver ode15i and the nonlinear least squares minimization is accomplished using the Levenberg-Marquardt algorithm as implemented in the Matlab function lsqnonlin.

5 Results and discussion

5.1 Objective Function

The proposed nonlinear fitting method involves the minimization of an objective function given by Equation 18. The rate of convergence, sensitivity to noise, and robustness of this procedure all depend on the behavior of the objective function for which the minimum is being sought. An example of the objective function is shown in Figure 2; the plot was created by generating synthetic data points of flame radius vs. time for $L_B = -1$ mm and $V_s^0 = 300$ mm/s and then evaluating the residual, Equation 18, for other values of the Markstein length and burning velocity. This residual (on a logarithmic scale) is indicated by the contours in Figure 2, and it is seen that the residual is minimized at the correct solution point. However the minimum in the objective function is rather elongated, that is, the solution point is much less sensitive to the Markstein length than to the unstretched burning velocity. Note that the apparent multiple local minima on the contour plot are artifacts of the contouring algorithm; the surface does in fact smoothly approach a single solution point.

Slices through the contour plot in Figure 2(a) for three values of the Markstein length are shown in Figure 2(b). In addition, noise in the experimental measurement of the flame radius has been simulated by adding random perturbations to each value of the flame radius; the magnitude of the added noise was take to be 0%, 1%, 2%, or 5% of the instantaneous flame radius. The objective function does exhibit a local minimum at the correct solution, but the depth of the minimum and the slope in its vicinity are reduced somewhat when noise is added. For the higher noise levels

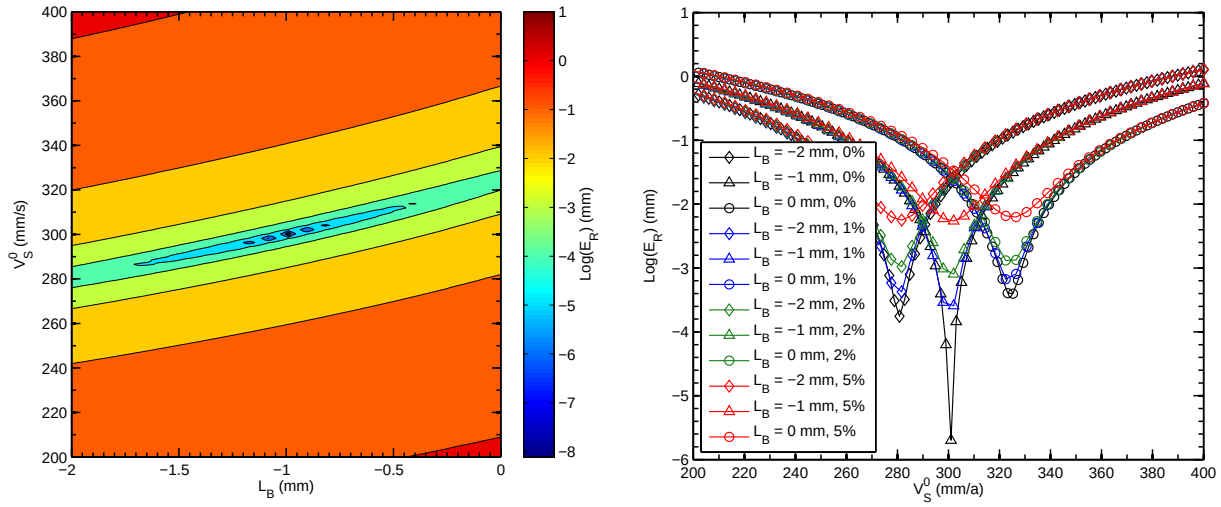

Figure 2: a) Contour plot of the objective function (Equation 18) for various values of Markstein length and unstretched burning velocity. The actual solution is $L_B = -1$ mm, $V_s^0 = 300$ mm/s. Contours levels are the base 10 logarithm of the objective function. b) Slices through the contour plot for Markstein lengths of -2, -1, and 0 mm. Random noise has been included by adding 0%, 1%, 2%, or 5% relative error to each flame radius data point.

the minimum is quite shallow; however, the nonlinear fitting method is still able to converge to the correct solution. Other noise models have also been employed including noise of uniform magnitude and noise that decreases with increasing flame radius; the results from those models were nearly indistinguishable from those shown in Figure 2(b).

The elongated shape of the minimum in the objective function is not a property of the new method alone, but is shared by both the linear method and the nonlinear method of Kelley and Law [19] (see section 2). These two methods also rely on least squares fitting by minimizing objective functions derived from Equation 9 and Equation 15, respectively. Contours of these two objective functions for the same conditions as Figure 2 are shown in Figure 3. Although the amplitudes of the residuals differ since each method minimizes a slightly different quantity, the qualitative behavior of all three methods is similar. Note, however, that the minimum for linear method deviates from the actual solution of $L_B = -1$ mm, $V_s^0 = 300$ mm/s because the flame is slightly outside of the linear stretch regime.

5.2 Performance of the present method

In order to evaluate the performance of the Levenberg-Marquardt, synthetic t_{syn} vs $R_{f,syn}$ data were generated using Equation 16 with L_B and V_S^0 values in the range $L_B \in [-5.0, L_{B,max}]$ mm where $L_{B,max} = \frac{R_f^0}{2e}$ and $V_S^0 \in [300, 35000]$ mm/s, which are representative of typical hydrocarbon-air and hydrogen-air mixtures. The choice of $L_{B,max}$ is based on the limit of Equation 16 described in section 3. After generating the synthetic data, an attempt was made to recover the laminar flame parameters from the synthetic data using a random set of initial guesses for L_B and V_S^0. The effect

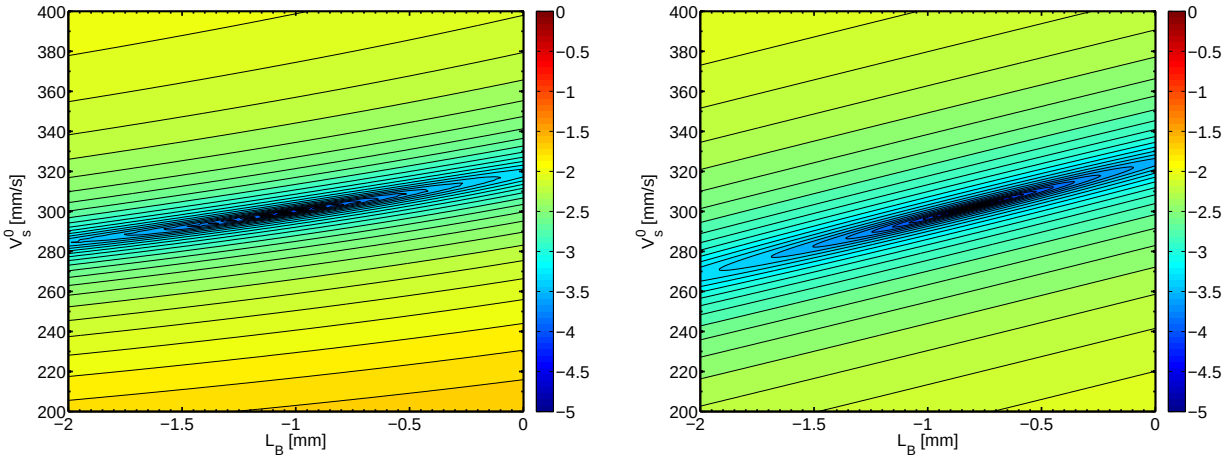

Figure 3: Contour plots of the objective function for Kelley and Law's method (left) and the linear method (right). The actual solution is $L_B = -1$ mm, $V_s^0 = 300$ mm/s.

of the number of points in the data set, the initial and final radii, and the initial guesses of L_B and V_S^0 on the performance of the method have been considered. In addition, noise was added to the synthetic data to assess its effect on the robustness of the method. The performance of the method is judged in terms of the final value of the residual, E_R, as well as in terms of the error of the fitted values of L_B and V_S^0. These errors are calculated using Equation 19 and Equation 20.

$$E_{V_S^0} = \frac{V_{S,syn}^0 - V_{S,calc}^0}{V_{S,syn}^0} \tag{19}$$

$$E_{L_B} = \frac{L_{B,syn} - L_{B,calc}}{L_{B,syn}} \tag{20}$$

Figure 4 shows examples of synthetic data sets characterized by positive Markstein lengths. The sets are generated using 100 points. In each case, both the correct values of the laminar burning speed and of the Markstein length were obtained by applying the non-linear least squares fitting procedure. The quality of the fitting is evident in the graphs presenting the evolution of the burning speed as a function of stretch rate.

5.2.1 Effect of data set properties

The effect on convergence was studied by varying parameters such as the initial flame radius, R_f^0, final flame radius, R_f^{final} and the size of the data set, N. To study the effect of N on convergence, data sets of t_{syn} vs $R_{f,syn}$ were generated based on the following parameters: $R_f^0 = 10$ mm, $R_f^{final} = 58$ mm, $N = [30, 50, 100]$. The N values represent typical data set sizes obtained from

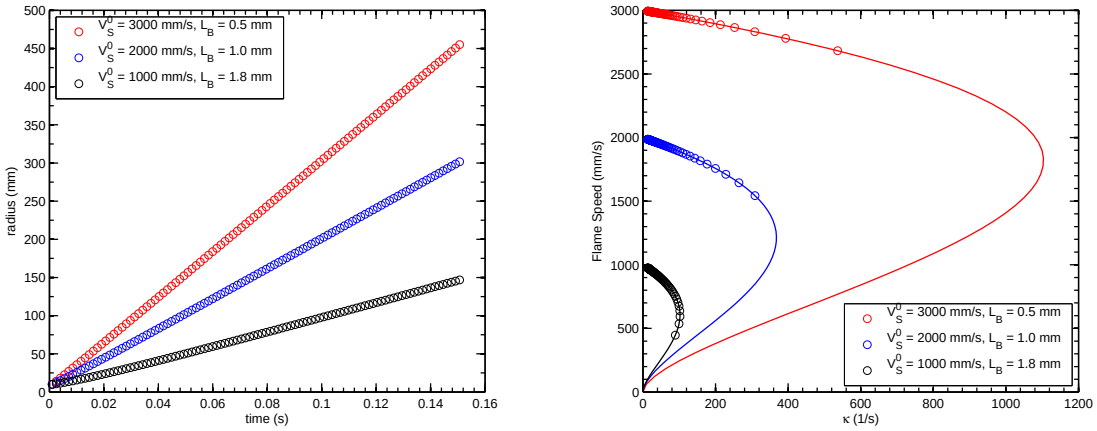

Figure 4: Examples of synthetic data and non-linear least-square regression curves obtained using the present numerical method. Both $R_{f,syn} = f(t_{syn})$ and $V_S^0 = f(\kappa)$ are presented.

experiments, where the size varies according to the framing rate of camera that is being used to acquire the flame images, the initial energy deposition used to ignite the mixture, and the type of mixture used; faster flames lead to less images and vice-versa. The non-linear least squares solver goes through 10 initial guesses of L_B and 10 initial guesses of V_S^0, until the residual, E_R, is minimized to the preset tolerance. The residual, E_R, and errors, $E_{V_S^0}$ and E_{L_B}, are shown in Figure 5 as filled contours on a base 10 logarithmic scale.

The results shown in Figure 5 suggest that E_R, $E_{V_S^0}$, and E_{L_B} are insensitive to the size of the data set, N. The figure also shows that E_R, $E_{V_S^0}$, and E_{L_B} increase near the region of $L_{B,max}$ indicated by the red contours, which is where the limit discussed in section 3 is approached. For the parameters tested, the results suggest that for the majority of Markstein lengths and flame speeds the non-linear least squares fitting procedure will perform within the desired tolerances.

Next the effect of initial radius is studied, keeping the number of points in the data set fixed at $N = 100$. Data sets of t_{syn} vs $R_{f,syn}$ were generated based on the following parameters: $R_f^0 = [10, 15, 25]$ mm, $R_f^{final} = 58$ mm. The non-linear least squares solver goes through 10 initial guesses of L_B and 10 initial guesses of V_S^0, until the residual, E_R, is minimized to the preset tolerance. The calculated errors, E_{L_B}, are shown in the left column of Figure 6 as filled contours on a base 10 logarithmic scale. The scale on the x-axis increases when R_f^0 increases since $L_{B,max}$ is directly proportional to the initial flame radius. Visually there are small differences in the magnitude of the contours of E_{L_B} for the $R_f^0 = 10$ mm and $R_f^0 = 15$ mm cases; the differences suggest that smaller errors are obtained for data sets with an initial flame radius of 10 mm than data sets with an initial flame radius of 15 mm. The 10 mm and 15 mm initial radius contours have a similar region of concentrated high errors in the vicinity of $L_{B,max}$. The 25 mm initial flame radius case exhibits a larger concentration of high errors in the vicinity of $L_{B,max}$ than the other two initial flame radius cases.

To study the effect of R_f^{final} on convergence, data sets of t_{syn} vs $R_{f,syn}$ were generated based on the following parameters: $R_f^0 = 10$ mm, $R_f^{final} = [25, 58, 80]$ mm. The non-linear least squares

solver goes through 10 initial guesses of L_B and 10 initial guesses of V_S^0, until the residual, E_R, is minimized to the preset tolerance. The calculated errors, E_{L_B}, are shown in the right column of Figure 6 as filled contours on a base 10 logarithmic scale. The scale on the x-axis remains fixed since R_f^0 is fixed for the three cases. There appears to be a change in the size of the region of concentrated high errors throughout the three cases. The size of the region decreases from the 25 mm final flame radius case to the 58 mm final flame radius case, it then increases again to a larger region of high errors in the 80 mm final flame radius case. Figure 6 suggests that there is an ideal final flame radius that leads to a decrease in the size of the region of concentrated errors in L_B.

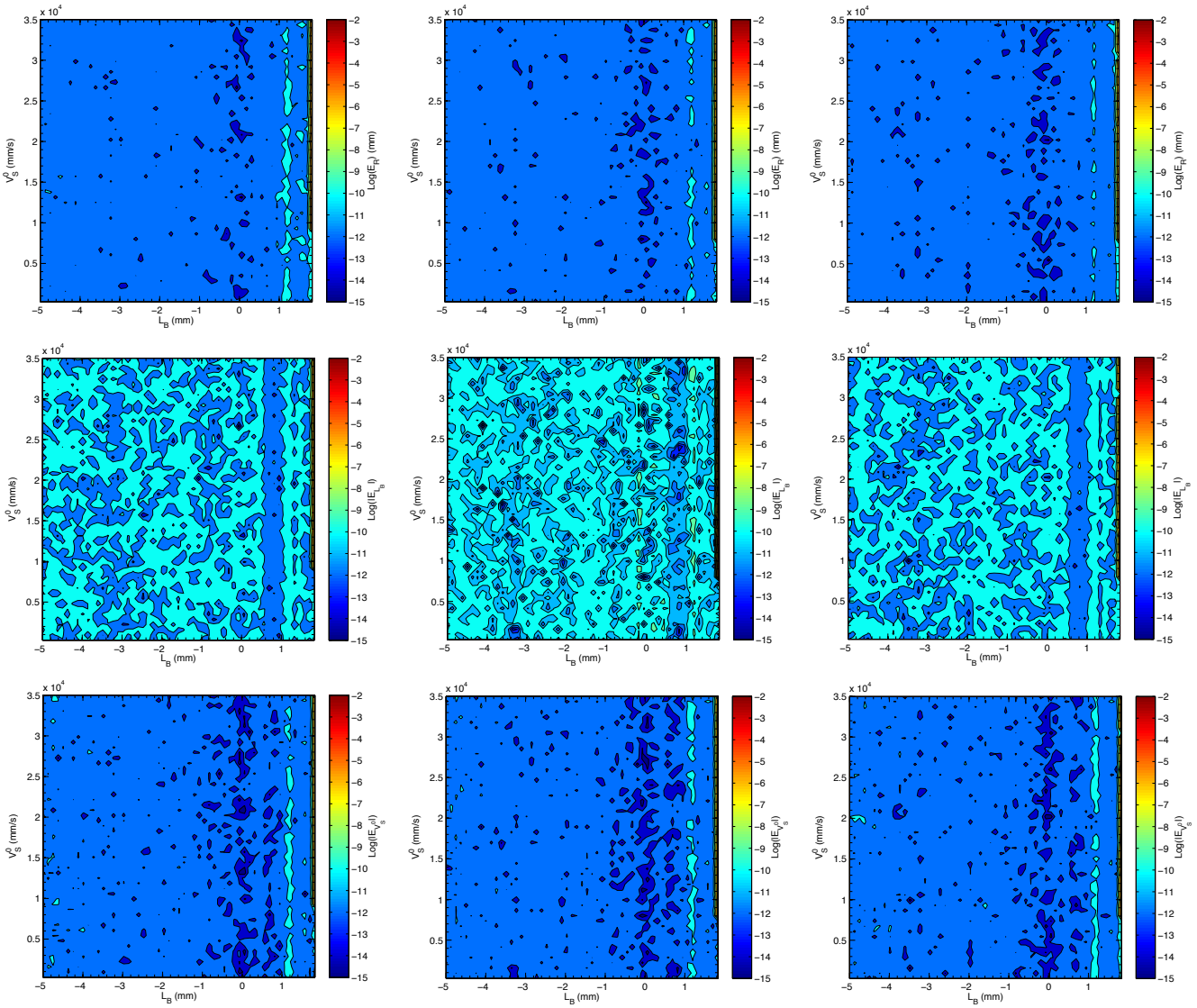

$N = 30$ $N = 50$ $N = 100$

Figure 5: Contour plots of E_R, E_{L_B} and $E_{V_S^0}$ for $N = [30, 50, 100]$

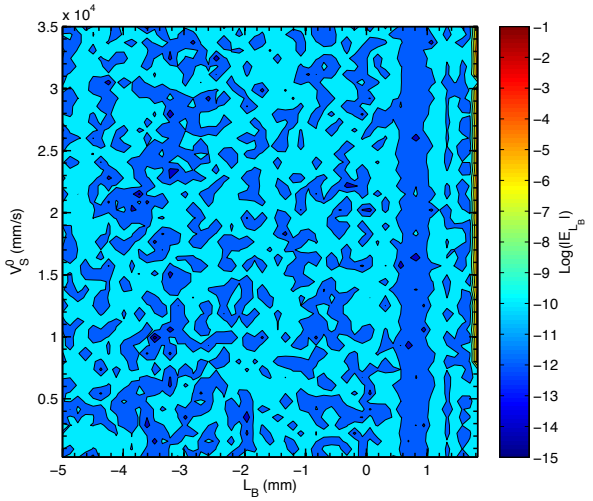

$R_f^0 = 10$ mm, $R_0^{final} = 58$ mm

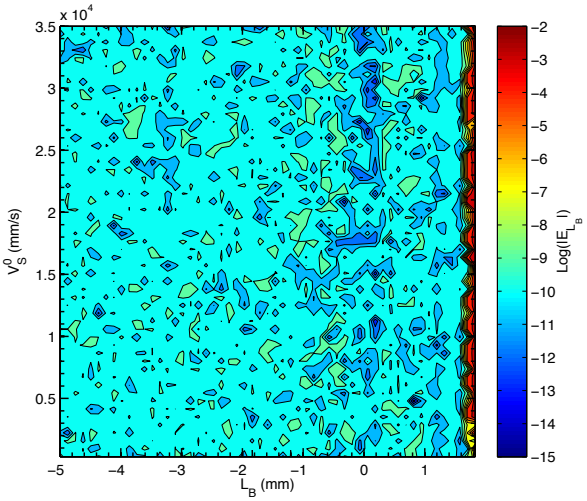

$R_f^0 = 10$ mm, $R_f^{final} = 25$ mm

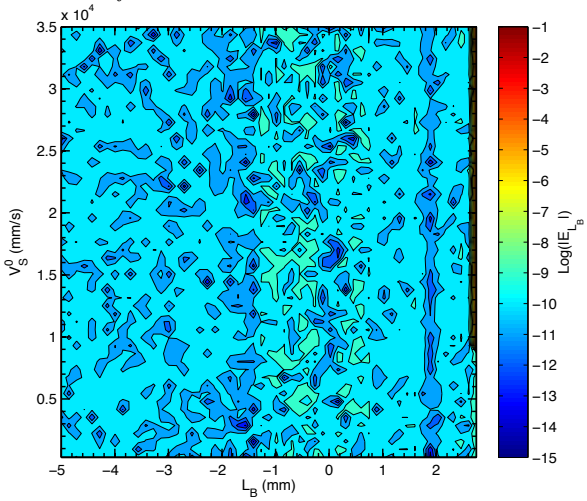

$R_f^0 = 15$ mm, $R_0^{final} = 58$ mm

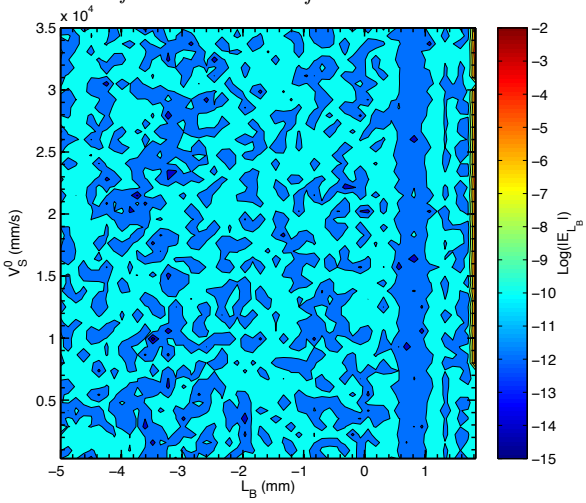

$R_f^0 = 10$ mm, $R_f^{final} = 58$ mm

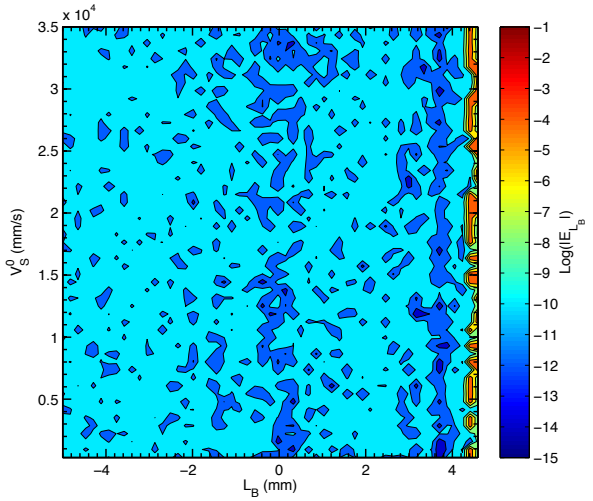

$R_f^0 = 25$ mm, $R_0^{final} = 58$ mm

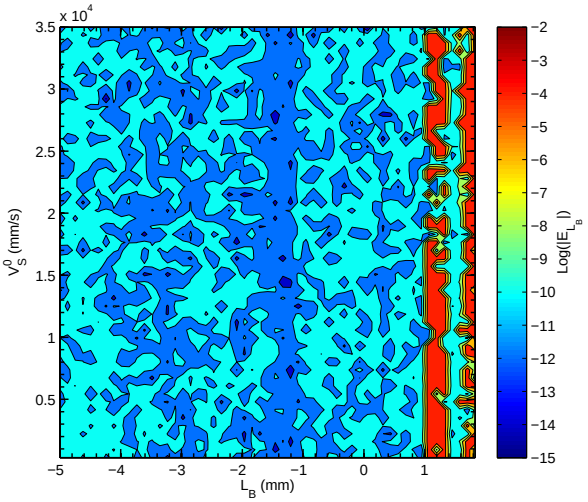

$R_f^0 = 10$ mm, $R_f^{final} = 80$ mm

Figure 6: Contour plots of E_{L_B} for various initial radii (left) and various final radii (right).

5.2.2 Effect of the initial guess

In this section the sensitivity of the nonlinear least squares fit to the initial guesses of L_B and V_S^0 is explored. Synthetic data sets were generated using initial and final radii of $R_f^0 = 10$ mm and $R_f^{final} = 58$ mm. The set of initial guesses was randomly generated for $L_B \in [-10, 10]$ mm and $V_S^0 \in [20, 100000]$ mm/s. For each pair of values of L_B and V_S^0, either 1, 2, 5, or 10 different initial guesses were used. The contour plots in Figure 7 indicate that when only 1 initial guess of L_B and 1 initial guess of V_S^0 are used, the error goes up as L_B increases until the non-linear least squares solver can no longer find a solution within a reasonable tolerance, this is indicated by the unfilled region of the 1×1 contour plot.

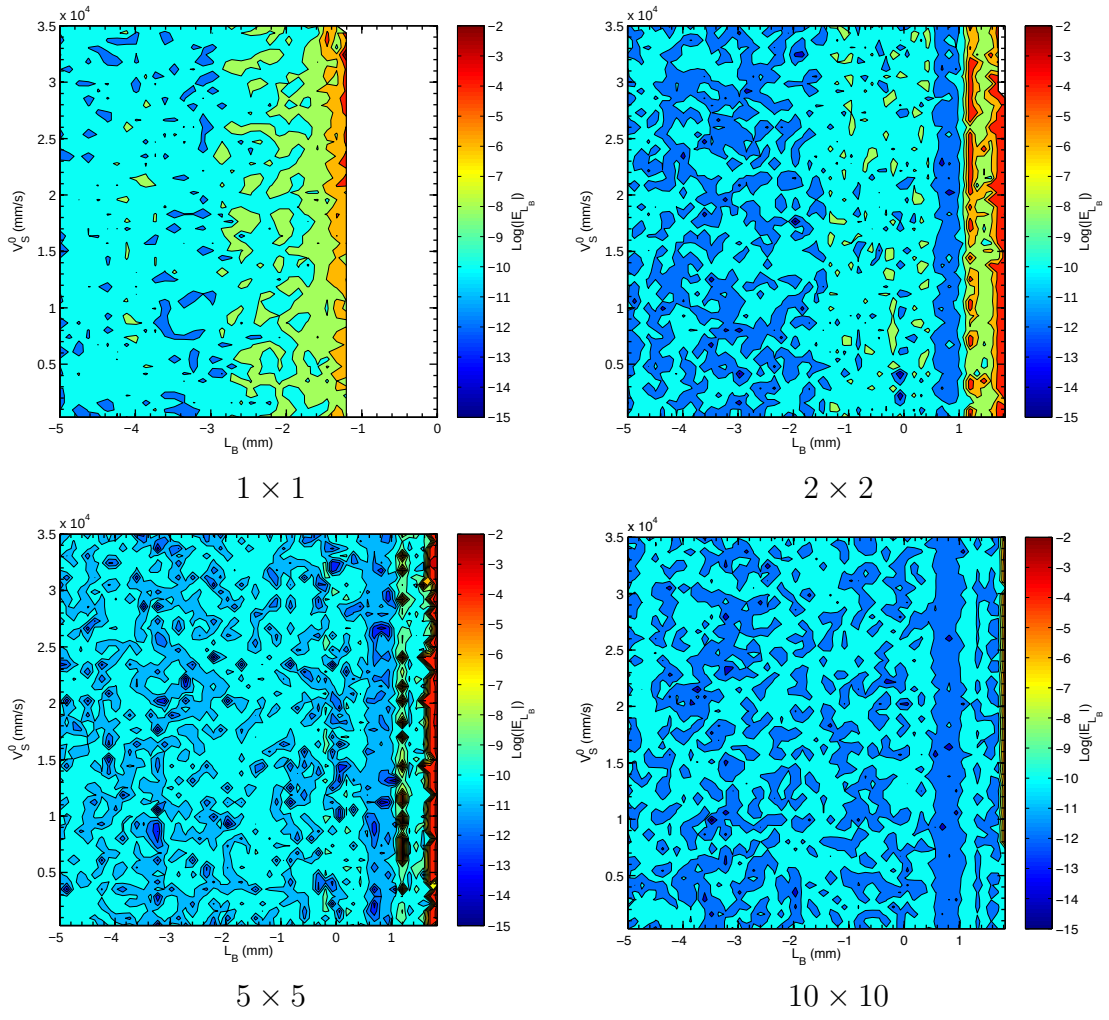

Figure 7: Contour plots of E_{L_B} for four sets of initial guessues of L_B and V_S^0

When the number of initial guesses is increased to 2 initial guesses of L_B and 2 initial guesses of V_S^0, the solver is able to find a solution within the preset tolerances for the majority of the

domain shown in the 2×2 contour plot. As the number of initial guesses is increased further, the magnitude of E_{L_B} decreases throughout the domain and the region of concentrated high errors becomes smaller, this is seen in the 5×5 and 10×10 contour plots in Figure 7. From this analysis, it is suggested that at least 10 initial guesses of L_B and 10 initial guesses of V_S^0 be chosen when using the non-linear least squares solver presented in this paper. If only 1 guess per parameter is to be used, then it is suggested that each guess be made on the basis of the linear least squares fit, Equation 9.

5.2.3 Effect of noise

The next step in this study was to investigate the robustness of the solver when noise was added to synthetic data of $R_{f,syn}$. The addition of noise to $R_{f,syn}$ is more representative of what is obtained experimentally when extracting flame radii from spherically propagating flame images. Data sets of t_{syn} vs $R_{f,syn}$ were generated based on the following parameters: $R_f^0 = 10$ mm, $R_f^{final} = 58$ mm. Noise proportional to the instantaneous flame radius was introduced to $R_{f,syn}$ via a noise vector, $\hat{e}$, that was randomly generated with values between -1 and 1. The resulting noisy synthetic data sets, $R_{f,i}$ are described by

$$R_{f,i} = R_{f,syn} * [1 + i * \hat{e}], \tag{21}$$

where i is the noise percentage. The addition of 1% and 2% noise were studied, and example flame radius plots are shown in Figure 8.

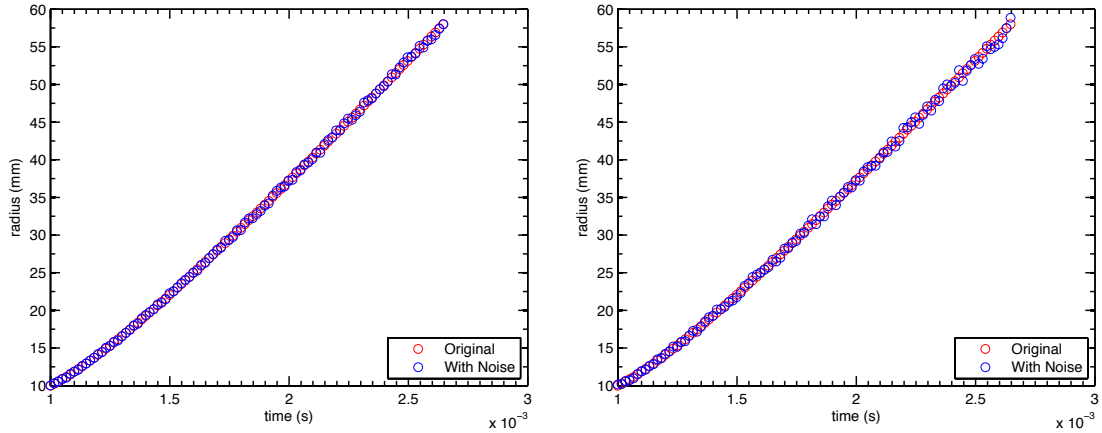

Figure 8: Exact solutions and solutions with 1% and 2% noise for a case with L_B = 1.8 mm and V_S^0 = 35000 mm/s.

The results of noise addition are shown in Figure 9, the figure is presented as synthetic L_B vs fitted L_B and the circle markers represent different values of V_S^0. The yellow markers indicate 0% noise addition, the red markers indicate 1% noise addition, the blue markers indicate 2% noise addition and the black dashed line indicates synthetic L_B = calculated L_B. Figure 9 shows that as the noise percentage is increased, the calculated L_B drifts further away from the synthetic L_B. In

addition, the calculated L_B drifts further away from the synthetic L_B as the value of the synthetic L_B decreases. However it should be noted that the error E_{L_B}, not shown, is evenly distributed in $L_B \in [-5.0, L_{B,max}]$ and $V_S^0 \in [300, 35000]$ mm/s for each noise addition case. These results show show that noisy data can lead to an uncertainty in the fitted Markstein length, especially for highly stretched flames. Nevertheless, the nonlinear search procedure performs well considering the shallowness of the least squares error minimum shown in Figure 2.

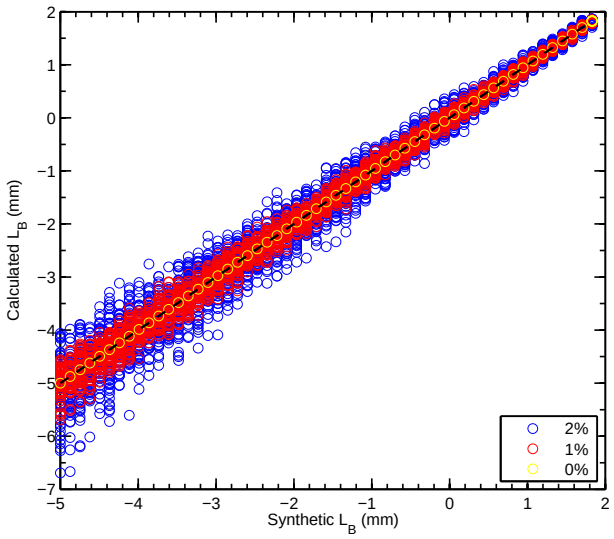

Figure 9: Synthetic L_B vs fitted L_B with 0%, 1%,and 2% added noise

Several of the cases reported above were repeated using the method of Kelley and Law [26] as well as the linear method. Typical results are shown in Figure 10, which mirrors the conditions of Figure 9. As would be expected, the linear method performs well only near conditions of zero stretch ($L/R_f \ll 1$) where the linearization is appropriate. The method of Kelley and Law on the other hand performs reasonably well over the entire range of Markstein lengths tested, with performance similar to that observed using the present method in Figure 9. In particular, the maximum deviation of the fitted Markstein length from the correct solution is about the same for both methods, as is the sensitivity to experimental noise. We have also found that the sensitivity of the method of Kelley and Law to other factors, such as the number of points in the data set and the choice of initial guess, is similar to that of the present method.

6 Conclusions

The performance of a nonlinear flame speed extraction method has been analyzed, and the sensitivity of the results to various experimental and numerical parameters has been explored. The results were found to be insensitive to the initial and final flame radius and the number of points in the data set. However, for positive Markstein length there is a minimum flame radius below which the nonlinear relationship between flame speed and stretch rate has no solutions, and the quality of the nonlinear fit can be poor as this limit is approached. Additionally, the fitted values of Markstein

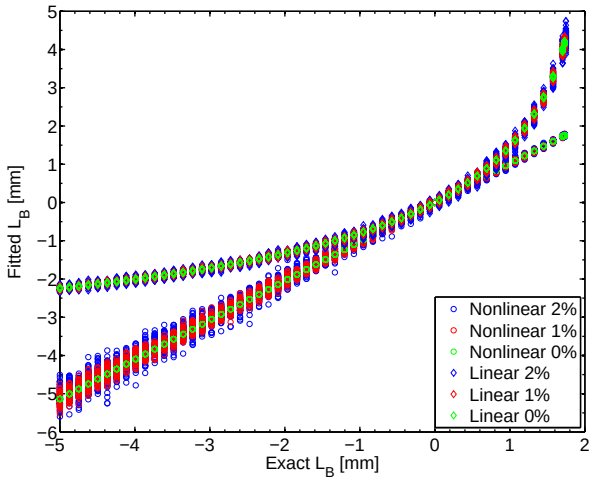

Figure 10: Comparison of synthetic L_B vs fitted L_B for 0, 1, and 2% added noise using the method of Kelley and Law as well as the linear fit. Initial flame radius is 10 mm, final radius is 58 mm, $N = 100$. For each value of L_b, the various points plotted correspond to different values of V_s^0 in the range (300,35000) mm/s.

length and laminar flame speed become more sensitive to their initial guesses near this limit. As a result, care should be taken that all data points used in the fit exceed this minimum radius.

The least squares error, which is minimized during the nonlinear fitting process, is found to exhibit a shallow minimum that depends only weakly on the Markstein length. When noise is added to the data, the local minimum becomes shallower and its depth is decreased. This can produce substantial errors in the fitted Markstein length, especially for highly stretched flames. The method used in this paper was compared with a similar nonlinear method developed by Kelley and Law [19], and similar performance was found in all aspects. In spite of the sensitivity to noise and the shallowness of the least squares minimum, these nonlinear methods performed considerably better than the linear method for highly stretched conditions.

References

[1] Z. Huang, Y. Zhang, K. Zeng, B. Liu, Q. Wang, and D. Jiang. *Combustion and Flame*, 146 (2006) 302–311.

[2] S. Bougrine, S. Richard, A. Nicolle, and D. Veynante. *International Journal of Hydrogen Energy*, 36 (2011) 12035–12047.

[3] I. Glassman. *Combustion.* Academic Press, Inc, Londres, 1987.

[4] J. Chomiak. *Combustion : a study in theory, fact and application.* Gordon and Breach Science Publishers, Suisse, 1990.

[5] T. Tahtouh, F. Halter, and C. Mounam-Rousselle. *Combustion and Flame*, 156 (2009) 1735–1743.

[6] O.C. Kwon and G.M. Faeth. *Combustion and Flame*, 124 (2001) 590–610.

[7] S. Jerzembeck, M. Matalon, and N. Peters. *Proceedings of the Combustion Institute*, 32 (2009) 1125–1132.

[8] S. P. M. Bane, R. Mével, S. A. Coronel, and J. E. Shepherd. *International Journal of Hydrogen Energy*, 36 (2011) 10107–10116.

[9] D.R. Dowdy, D.B. Smith, Taylor S.C., and A. Williams. *Proceedings of the Combustion Institute*, 23 (1990) 325–332.

[10] G.H. Markstein. *Journal of the Aeronautical Sciences*, 18 (1951) 199–209.

[11] G.I. Sivashinsky. *Acta Astronautica 3 (1976)*, 3 (1976) 889–918.

[12] M. Matalon and B.J. Matkowsky. *Journal of Fluid Mechanics*, 124 (1982) 239–259.

[13] P. Clavin. *Progress in Energy and Combustion Science*, 11 (1985) 1–59.

[14] K.T. Aung, M.I. Hassan, and G.M. Faeth. *Combustion and Flame*, 109 (1997) 1–24.

[15] K.T. Aung, L.K. Tseng, M.A. Ismail, and G.M. Faeth. *Combustion and Flame*, 102 (1995) 526–530.

[16] R. Mével, F. Lafosse, N. Chaumeix, G. Dupré, and C.-E. Paillard. *International Journal of Hydrogen Energy*, 34 (2009) 9007–9018.

[17] N. Lamoureux, N. Djebali-Chaumeix, and C.E. Paillard. *Experimental Thermal and Fluid Science*, 27 (2003) 385–393.

[18] P. Ronney and G. Sivashinsky. *SIAM Journal of Applied Mathematics*, 49 (1989) 1029–1046.

[19] A.P. Kelley and C.K. Law. *Combustion and Flame*, 156 (2009) 1844–1851.

[20] F. Halter, T. Tahtouh, and C. Mounam-Rousselle. *Combustion and Flame*, 157 (2010) 1825–1832.

[21] A. P. Kelley, A. J. Smallbone, D. L. Zhu, and C. K. Law. *Proceedings of the Combustion Institute*, 33 (2011) 963–970.

[22] N. Bouvet, C. Chauveau, I. Gkalp, and F. Halter. *Proceeddings of the Combustion Institute*, 33 (2011) 913–920.

[23] E. Varea, V. Modica, A. Vandel, and B. Renou. *Combustion and Flame*, 159 (2012) 577–590.

[24] B. Karlovitz, J.R. Denission, D.H. Knapschaffer, and F.E. Wells. *Proceedings of the Combustion Institute*, 4 (1953) 613–620.

[25] D. Bradley, P.H. Gaskell, and X.J. Gu. *Combustion and Flames*, 104 (1996) 176–198.

[26] A.P. Kelley and C.K. Law. *Combustion and Flame*, 156 (2009) 1844–1851.

[27] Z. Chen. *Combustion and Flame*, 158 (2011) 291–300.